ACS central science

http://pubs.acs.org/journal/acscii

Research Article

Polyethylenimine–Poly(lactic-*co*-glycolic acid)$_2$ Nanoparticles Show an Innate Targeting Ability to the Submandibular Salivary Gland via the Muscarinic 3 Receptor

Junchao Xu,[#] Kaiwei Wan,[#] Hui Wang, Xinghua Shi, Jing Wang, Yi Zhong, Chao Gao, Yinlong Zhang,* and Guangjun Nie*

Cite This: *ACS Cent. Sci.* 2021, 7, 1938–1948

Read Online

ACCESS | Metrics & More | Article Recommendations | Supporting Information

ABSTRACT: Polymeric nanoparticles have been extensively explored for biomedical applications, especially as framework materials for the construction of functional nanostructures. However, less attention has been paid to the inherent biological activities of those polymers. In this work, one of the commonly used polymers in gene and protein delivery, polyethylenimine–poly(lactic-*co*-glycolic acid)$_2$ (PEI–PLGA), was discovered by accident to be able to mediate the nanoparticles to target the submandibular salivary glands of mice after intravenous injection. PEI–PLGA nanoparticles with an unmodified PEI surface selectively accumulated in submandibular salivary glands with *ex vivo* and *in vitro* study, suggesting that a ligand–receptor interaction between PEI and muscarinic acetylcholine receptor subtype 3 (M3 receptor) contributed to this affinity. Docking computation for the molecular binding mode between PEI segments and M3 receptor indicated the way they interacted was similar to that of the FDA-approved specific M3 receptor antagonist, tiotropium. The key amino acids mediated this specific interaction between PEI–PLGA nanoparticles and M3 receptor were identified via a simulated alanine mutation study. This work demonstrates the unique characteristic of PEI–PLGA nanoparticles, which may be useful for the development of muscarinic receptor targeted nanomedicines and should be taken into consideration when PEI-based nanoparticles are applied in gene delivery.

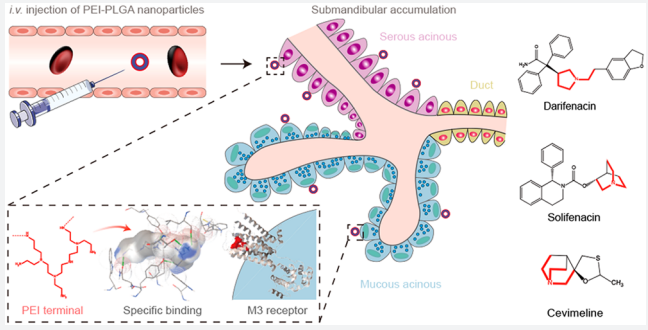

INTRODUCTION

The tissue-specific targeting of drug delivery systems has become a central challenge in drug delivery and nanomedicines.[1] During the past decades, increasing efforts have been dedicated to improving the selectivity of conventional nanomedicines and to developing new targeting strategies.[1−3] To date, most of the nanomedicines devised for tissue-specific delivery apply targeting ligands to recognize receptors on tissue specific cells or extracellular components. Numerous novel ligands, including antibodies, peptides, DNA/RNA aptamers, and polysaccharides, have been reported either covalently conjugated or noncovalently attached onto a nanoparticle surface.[4−8] While this common practice allows great versatility in nanomedicine design and functionalization, such incorporation of additional ligands, often biological macromolecules themselves, into a delivery system also introduces additional complexity with high cost. In fact, most of the heretofore commercially available nanomedicines have used simple polymeric or liposomal vehicles without any introduction of targeting ligands, and nanomedicines with complicated design are often related to limited scalability in standardized production and therefore have a difficult translation into clinical use.[9−11] Meanwhile, intrinsic properties of commercially applied nanoparticles require more detailed exploration.

In response to this challenge, an emerging direction in nanomedicine designed to exploit unmodified nanoparticles with intrinsic biological activities has been proceeding in order to reduce the further processing needed for the final nanomedicine to achieve some favorable features such as targeting ability, stimuli-responsiveness, or therapeutic activity. Since such innate activity often depends on a specific molecular interaction with biological systems, materials based on biological macromolecules such as peptides,[7] nucleic acids,[5,12,13] or proteins[6] are often seen as ready choices for this type of strategy. In recent years, it has come to our attention that several synthetic polymers also possess useful biological functions or can acquire them through precise

Received: September 5, 2021
Published: November 4, 2021

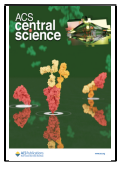

https://doi.org/10.1021/acscentsci.1c01083
ACS Cent. Sci. 2021, 7, 1938–1948

Scheme 1. PEI−PLGA Nanoparticles Accumulate in the Submandibular Gland by Targeting the M3 Receptor via the Shared Triethylamine Group[a]

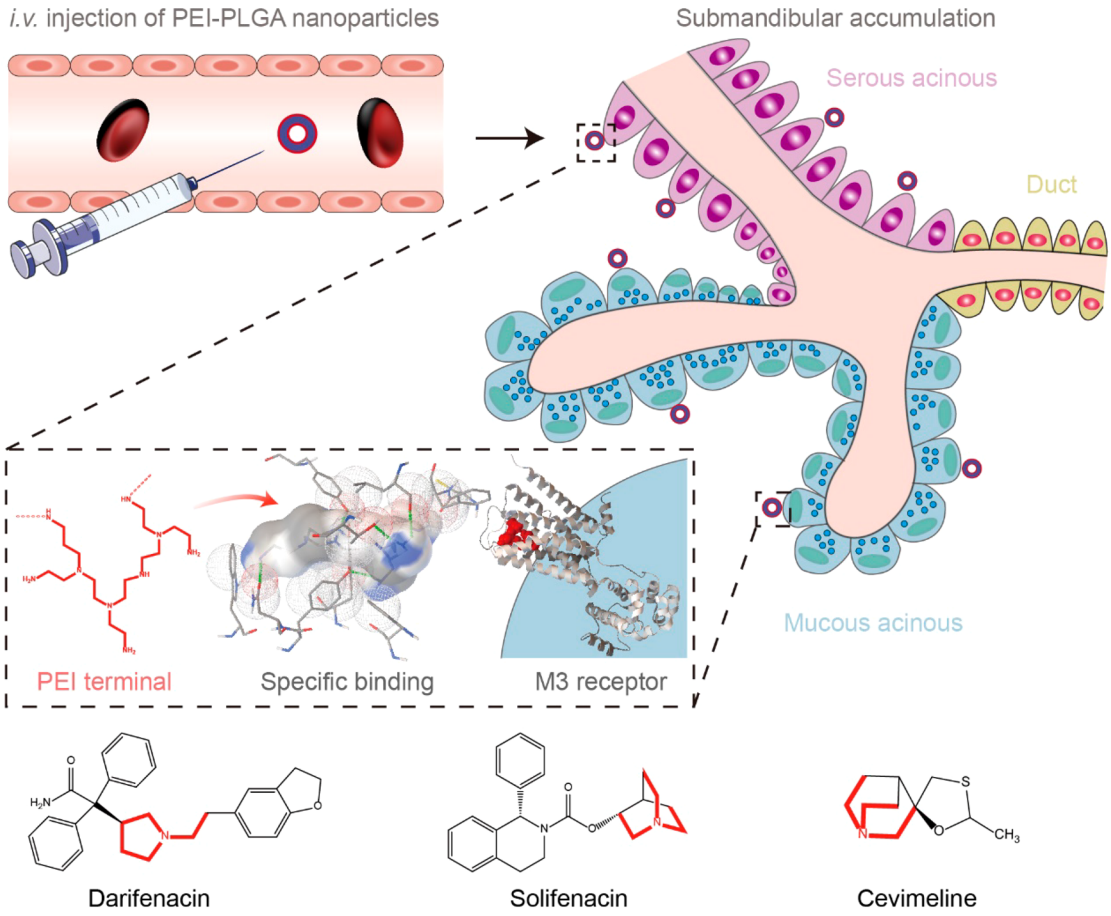

[a]The PEI−PLGA nanoparticles strongly accumulate in the submandibular glands of mice after tail vein injection. The abundant tertiary amine (triethylamine) groups present in the PEI polymer, in common with most of the reported M3 receptor-binding drugs, imply a molecular basis for this affinity. The molecular structure of several M3 receptor antagonists or agonists is shown.

chemical modification.[14] These polymers typically contain particular moieties that can selectively interact with their targets to interfere with their function, such as the poly(ethylene glycol) functionalization of the fourth generation of poly(acyl thiourea) dendrimer with antiangiogenesis and anticancer activities.[2,14−16] Given that polymeric nanoparticles are currently one of the most widely used category of drug carriers, the development of polymeric nanomaterials with innate tissue-targeting capacity would certainly be of great interest, not only for the development of simpler and cheaper drug delivery systems but also for the possibility to reveal novel principles and strategies for nanomedicine design in the future. However, this requires profound understanding about the interactions of polymeric nanostructures with cells, proteins, and other biological components of which the current knowledge and research is still lacking, especially on the molecular level.

In this work, we reported that unmodified polyethylenimine−poly(lactic-*co*-glycolic acid)$_2$ (PEI−PLGA) nanoparticles with the hydrophilic PEI fully exposed on the surface around the aqueous phase were capable of selectively accumulating in the submandibular salivary glands in mice through a high affinity with acetylcholine receptors in the specific tissue, similar to most of the FDA-approved muscarinic acetylcholine receptor subtype 3 (M3 receptor)-binding drugs (e.g., darifenacin, tiotropium, and cevimeline) in the structure (Scheme 1). With its cationic surface, the PEI−PLGA nanoparticle is capable of adsorbing many negatively charged biological molecules including RNA, protein, and DNA and has already been widely used for delivery of nucleic acid or protein drugs[17−19] simply via nonselective static electric attraction. Our study, however, suggests that being mediated by its triethylamine groups, PEI could interact in a particular manner with M3 receptor, a type of acetylcholine receptor abundantly expressed around the outside of the acinus in the submandibular salivary glands. Using docking computation and alanine mutation simulation, we have also identified the key amino acids (including Tyr529, Tyr148 and Tyr506, Asp147 and Trp503) in the M3 receptor protein that may have participated in the interaction with the periphery of the PEI chain. These findings may provide insights into the biological application of synthetic polymers and highlight the potential of polymer−protein computation methods in nanomedicine design. Moreover, these results may also be useful for the development of M3 receptor-targeted nanomedicines to treat related diseases.

RESULTS AND DISCUSSION

PEI−PLGA Nanoparticles Selectively Accumulated in Submandibular Salivary Glands of Mice after Intra-

https://doi.org/10.1021/acscentsci.1c01083
ACS Cent. Sci. 2021, 7, 1938−1948

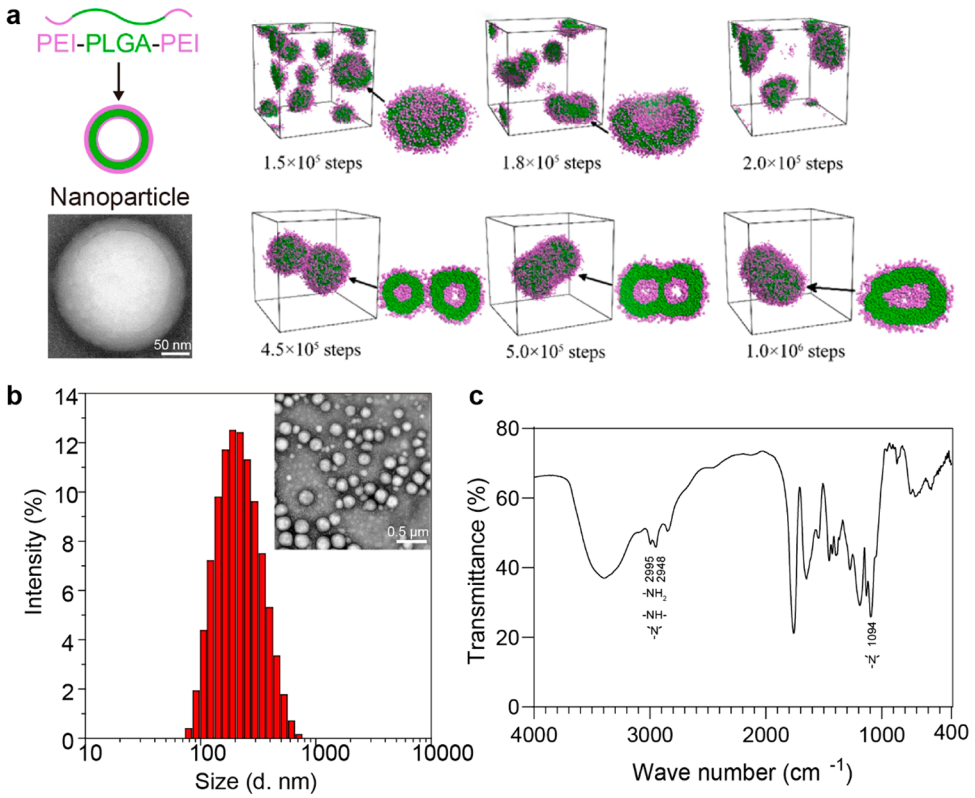

Figure 1. Characterization of PEI−PLGA nanoparticles. (a) Dissipative particle dynamics simulation of the PEI−PLGA nanoparticles using a coarse-grained PEI−PLGA copolymer model (pink beads: PEI; green beads: PLGA). Branched PEI was presented on the surface of the assembled PEI−PLGA nanoparticles in the aqueous phase. (b) The morphology (inset image) and size distribution of the PEI−PLGA nanoparticles. (c) Infrared spectroscopy of the lyophilized PEI−PLGA nanoparticles showed the presence of the typical triethylamine group in branched PEI.

venous Administration. The model nanomaterial selected in this study was the commonly used polyethylenimine−poly-(lactic-*co*-glycolic acid)$_2$, designated as PEI−PLGA, nanoparticles, prepared by a double emulsion method, which was similar to our previous study.[20] First, dissipative particle dynamic simulation was performed to generate a good knowledge of the PEI−PLGA nanoparticle's microstructure, and we found that its surface was dominated by PEI segments in an aqueous environment (Figure 1a).[21] Amphiphilic PEI−PLGA triblock copolymer molecules were allowed to self-assemble in a water/oil/water (W/O/W) emulsion into spherical nanoparticles with the cationic PEI block on the surface. Under a physiological pH (~7.4) environment, the product particles had an average hydrodynamic diameter of approximately 210.1 nm and zeta potential of 44 mV (Figure 1b and Table S1), indicating the protonation of the PEI termini, and the hydrodynamic diameter remained stable in PBS within 4 days after preparation (Table S2). Infrared spectra validated the existence of the triethylamine group in the PEI−PLGA nanoparticles (Figure 1c). However, the zeta potential decreased to −15 mV at pH = 10 to guarantee the complete neutralization of protons on the cationic surface. PEG−PLGA nanoparticles with a similar structure were also prepared as the control (Table S1), which exhibited high structural similarity with the PEI−PLGA nanoparticles and were also most commonly used for drug delivery.

The tissue distribution profile of both PEI−PLGA and PEG−PLGA nanoparticles labeled with Rhodamine B in BALB/c mice after intravenous administration was investigated by fluorescence imaging. After administration of different nanoparticles for 8 h, major organs of the mice were excised for *ex vivo* imaging (Figure 2a). Despite the difference in surface charge, both nanoparticles showed a similar distribution in most tissues investigated, including notable retention in the liver, presumably due to clearance by the mononuclear phagocytic system. However, PEI−PLGA nanoparticles demonstrated significantly enhanced accumulation in the submandibular salivary glands of mice compared to PEG−PLGA particles (Figure 2a,b). Ultrathin sections of nanoparticle-treated submandibular glands examined by transmission election microscopy (TEM) further indicated that the PEI−PLGA nanoparticles were trapped around both the serous alveoli and mucous alveoli in the tissue (Figure 2c), confirming this increased accumulation *in vivo*. In contrast, hardly any PEG−PLGA nanoparticles were identified in the submandibular glands.

Further investigation revealed a probable affinity of PEI−PLGA nanoparticles to the muscarinic M3 acetylcholine receptor, a central mediator of submandibular salivary secretion highly expressed in both mouse and human submandibular salivary glands. M3 receptor proteins in the excised glands were stained with an Alexa Fluor 488 conjugated M3 antibody to determine its colocalization with nanoparticle-encapsulated Rhodamine B. In the examined tissues, both the substructures of acinus (bubble shape with loose nucleus distribution) and ducts (tube shape or bubble shape with compact nucleus distribution when sliced in cross sections) showed strong M3 receptor expression around the surface. Notably stronger colocalization between the Alexa Fluor 488 and Rhodamine B fluorescent channels was in fact

https://doi.org/10.1021/acscentsci.1c01083
ACS Cent. Sci. 2021, 7, 1938−1948

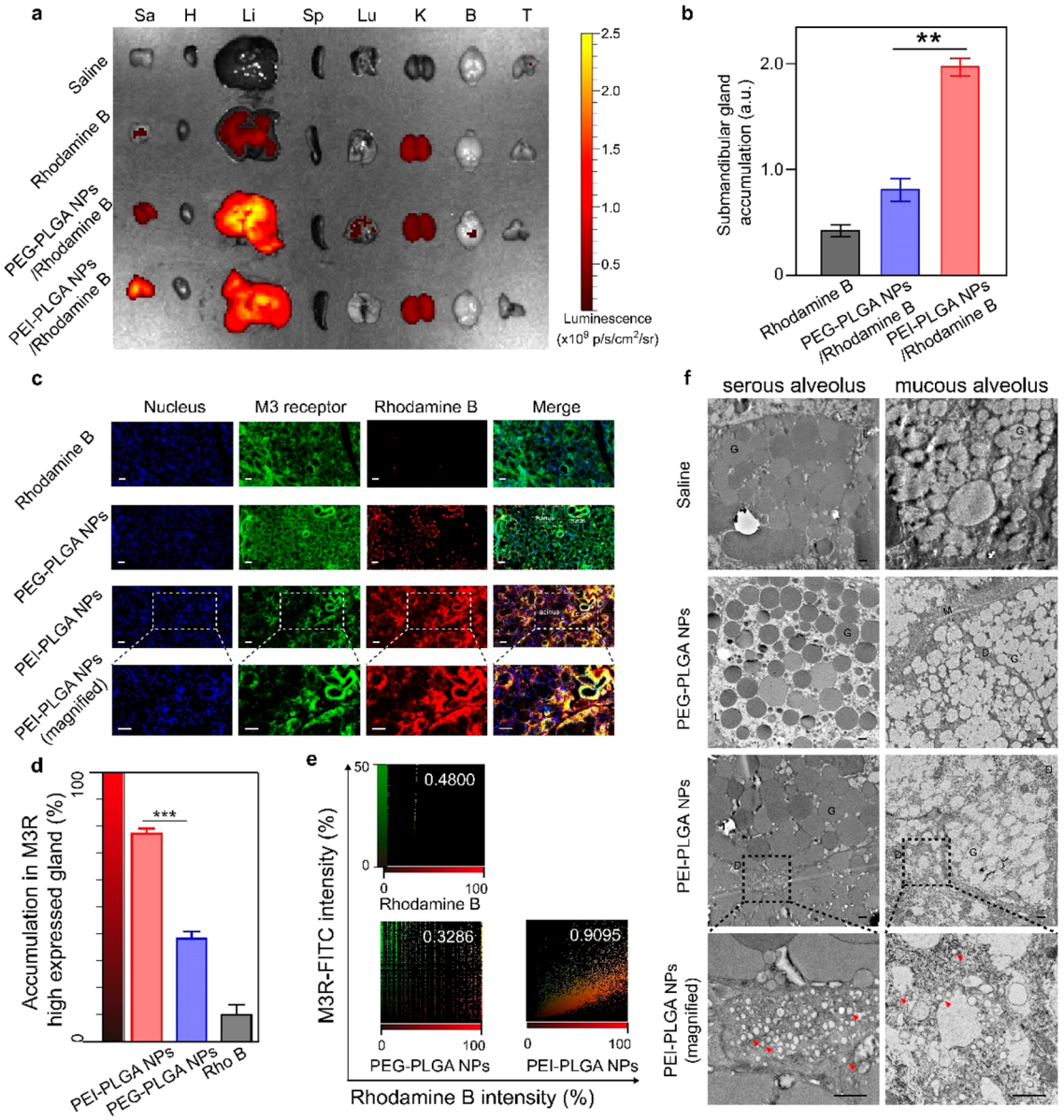

Figure 2. PEI−PLGA nanoparticles selectively accumulated in the submandibular salivary glands of mice. (a) Representative *ex vivo* imaging results of different organs derived from mice administered with free Rhodamine B dye and Rhodamine B labeled nanoparticles through the tail vein (8 h postinjection). Sa, submandibular salivary gland; H, heart; Li, liver; Sp, spleen; Lu, lung; K, kidney; B, the whole brain; T, thymus gland. (b) Fluorescence quantification of Cy5.5-labeled nanoparticles in the submandibular gland (n = 3). (c) Representative fluorescence visualization of the frozen sections of the submandibular salivary gland tissues derived from mice treated as in (a) (scale bar, 20 μm) with quantification of Rhodamine B intensity (d) in form of relative percentage, n = 3. The results are shown as mean ± SD. (e) Fluorescent intensity plot charts derived from the results in (c) showing the degree of colocalization between nanoparticle-delivered Rhodamine B and M3 receptor staining signals. The parameter on the top right corner of each plot indicated Pearson correlation coefficients, which reflect the strength of positive correlation between the two channels. (f) Representative TEM images of ultrathin sections of submandibular salivary glands showing the serous alveolus and mucous alveolus areas. G, secretory granules; D, ducts; M, myoepithelium. Scale bar, 1 μm. **p < 0.01; ***p < 0.001.

visualized in the PEI−PLGA nanoparticle treated tissue in comparison to the PEG−PLGA treated group (Figure 2d,e). The Pearson's correlation coefficient of the PEI−PLGA group was 0.9095, significantly higher than that of PEG−PLGA (0.3286), showing the strong colocalization relationship between the M3 receptor expression and the PEI−PLGA accumulation, while the PEG−PLGA group showed random and low distribution among the submandibular salivary independent of the M3 receptor expression (Figure 2f). These results further suggested that the specifically enhanced retention of the PEI−PLGA nanoparticles in the mouse submandibular salivary glands was at least partially associated with the abundance of the M3 receptor therein. Although submandibular salivary glands were not the only type of organ with high M3 receptor expression, it was also possible that their anatomical location and structure was particularly favorable for the retention of intravenously injected nanostructures. For example, in an RNA sequencing study of M3 receptor from 20 human tissues, other than the submandibular salivary gland showing the highest RPKM (reads per kilobase per million mapped reads) at 1.129, the second highest was the whole brain (RPKM = 1.001).[22] This result basically

https://doi.org/10.1021/acscentsci.1c01083
ACS Cent. Sci. 2021, 7, 1938−1948

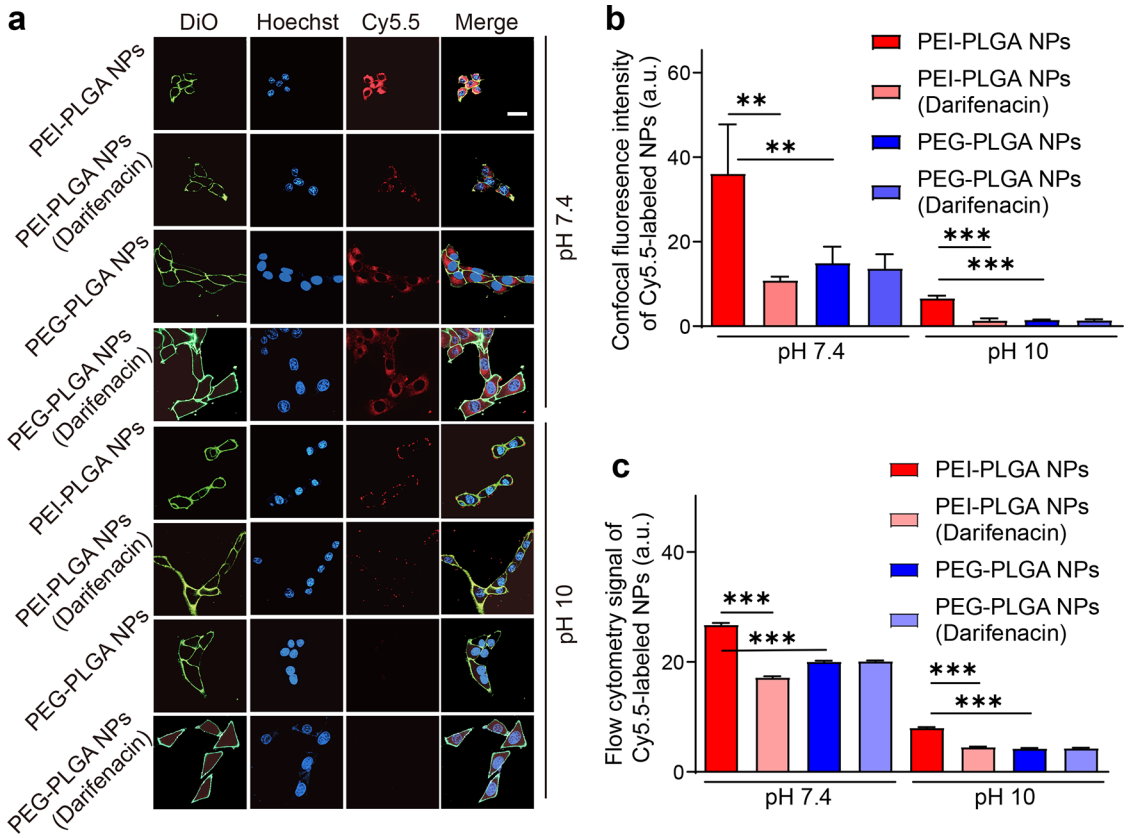

Figure 3. Enhanced affinity of PEI−PLGA nanoparticles with high M3 receptor expression cell line bEnd.3. (a) Representative confocal images of bEnd.3 cells after 0.5 h of coincubation with Cy5.5-labeled nanoparticles. Darifenacin pretreatment was applied to inhibit M3 receptor function. Scale bar, 10 μm. (b) Confocal fluorescent intensity quantification of Cy5.5-labeled nanoparticles (n = 3). (c) Cellular fluorescence intensity of bEnd.3 cells after 0.5 h of coincubation with Cy5.5-labeled nanoparticles analyzed by a flow cytometry assay (n = 5). **p < 0.01; ***p < 0.001.

corresponded to the M3 receptor expression level in mouse tissue (Figure S2) as well as the neurological effects of the M3 receptor.[23−26] However, the whole brain was likely not accessible to the injected positively charged PEI−PLGA nanoparticles through the compact blood brain barrier.[27]

PEI−PLGA Nanoparticles Showed Specific Affinity with M3 Receptor Positive Cells. To further investigate the interaction between the M3 receptor and the PEI-based nanoparticles, cellular binding tests were carried out for PEI−PLGA and PEG−PLGA nanoparticles *in vitro*. bEnd.3 was selected for the subsequent experiments for its particularly high M3 receptor expression (Figure S3).[28] The cells were incubated with either PEI−PLGA nanoparticles or PEG−PLGA nanoparticles for 30 min at 4 °C to slow down their internalization. Confocal microscopy analysis demonstrated that, at physiological pH (7.4), the cellular association of the PEI−PLGA nanoparticles was in fact significantly stronger compared to that of the PEG−PLGA nanoparticles (Figure 3a,b), consistent with their higher submandibular salivary gland accumulation. However, when PEI−PLGA nanoparticles were incubated with bEnd.3 cells pretreated (1 h) with darifenacin, an M3 receptor antagonist, their association with the cells diminished greatly, presumably due to the competition binding between darifenacin and the M3 receptors.[29] In contrast, no significant change was detected in the cellular affinity of the PEG−PLGA nanoparticles when coincubated with darifenacin-treated cells. This selective blocking effect on the cellular binding of the PEI−PLGA nanoparticles through M3 inhibition was then confirmed by the highly similar trends observed in a flow cytometry assay (Figure 3c). From these data, we conclude that M3 receptors may indeed have an important contribution to the enhanced bEnd.3 cell association of PEI-based nanoparticles over PEG-based ones. On the basis of the previous studies, the PEI segments were endowed with a different protonation rate according to the environmental pH.[30] Briefly, full deprotonation happens in an alkaline condition (pH ∼ 10.0) while all primary amines of branched PEI are protonated at physiological pH around 7.4. To exclude the electrostatic adsorption effect of PEI with the cell membrane, the same analysis was performed under pH 10.0 in order to deprotonate the tertiary amine groups on the PEI surface; the cellular association of PEI−PLGA nanoparticles still remained significantly higher (∼2-fold) than the PEG−PLGA control and sensitive to the antagonization of the M3 receptor by darifenacin, even if the total cellular associated signals in each group became much weaker (Figure 3a−c). It should be noted that the signals of negatively charged PEG−PLGA particles were similarly truncated, possibly indicating that the compromised uptake function of the cells under unfavorable pH also played a decisive role in this change. In fact, according to confocal visualization (Figure 3a), at pH 10, almost no fluorescence signal was observed within the cytoplasm, while at pH 7.4, both PEI−PLGA and PEG−PLGA nanoparticles showed strong internalization during the same time period. When quantified by flow cytometry (Figure 3c), the association of the PEI−PLGA nanoparticles with darifenacin-treated bEnd.3 cells was close to that of the PEG−PLGA

https://doi.org/10.1021/acscentsci.1c01083
ACS Cent. Sci. 2021, 7, 1938−1948

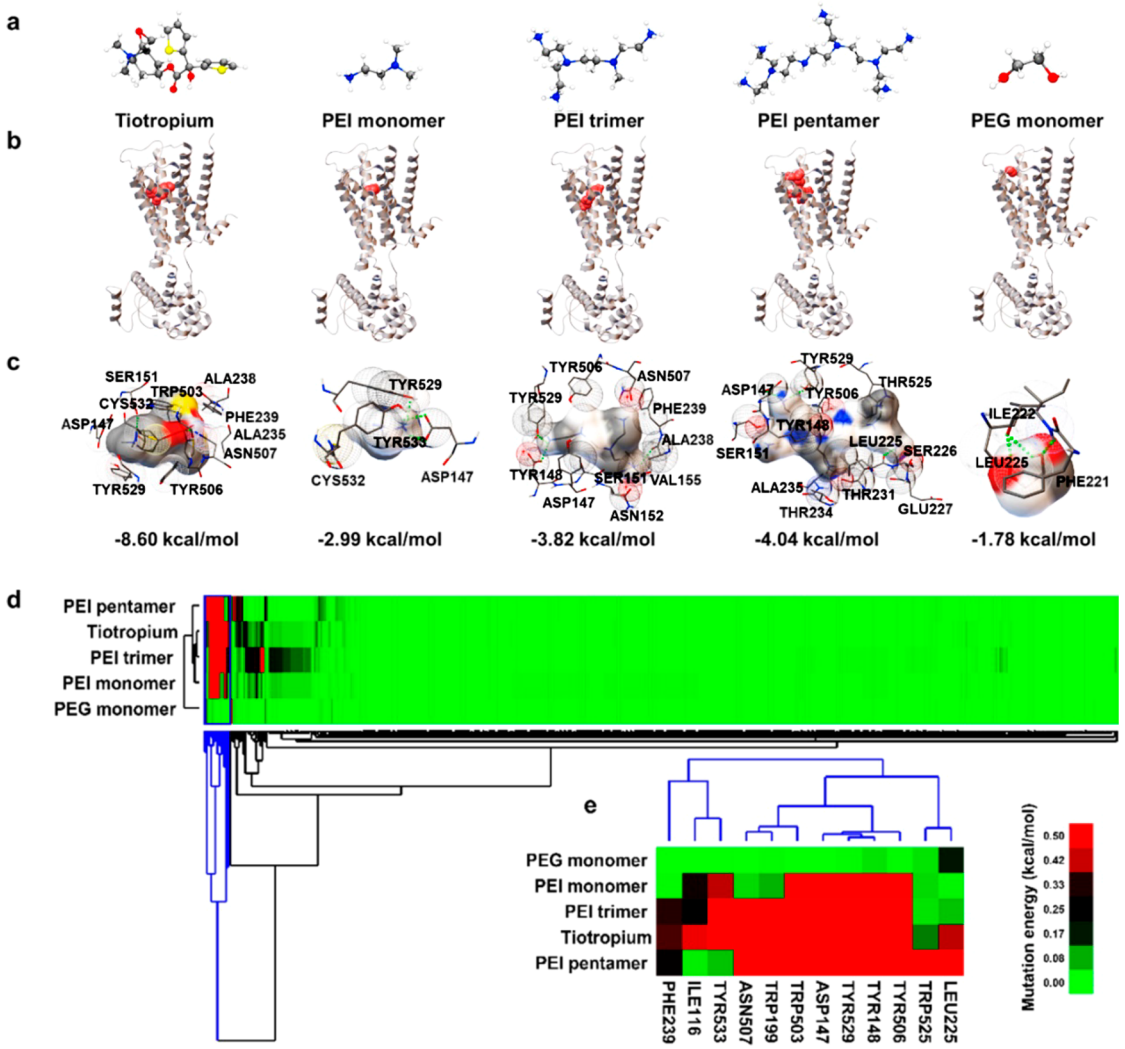

Figure 4. Analysis of the interaction between ligands (tiotropium, PEI segments, and PEG segment) and the M3 receptor. (a) Optimized molecular structures of tiotropium, PEI monomer, PEI trimer, PEI pentamer, and PEG monomer (atom color: C, gray; H, white; N, blue; O, red; S, yellow). (b) Predicted binding modes of the M3 receptor with the five compounds in (a). (c) Binding interaction between the five compounds and the amino acid residues of the M3 receptor, where the green dotted lines represent the H bond interaction. (d) Alanine scanning mutagenesis simulation results for all 428 amino acids on the M3 receptor monomer, where the mutation energy level was visualized using a heat map. Cluster analysis with all groups of mutation energy was carried out by the k-means method. The blue-lined cluster indicates the specific amino acids group with the most significant change in mutation energy. (e) Enlarged presentation of the blue-lined cluster in (d), highlighting the similarity among mutation energy profiles of the PEI segments and tiotropium.

nanoparticles, which further implied that the nonspecific adsorption of the PEI-based particles due to their surface charge could not fully account for their observed high cell affinity. Finally, another cell line with positive but lower M3 receptor expression (Figure S3), human umbilical vein endothelial cells (HUVECs), was also subjected to the same experiments for comparison. The results demonstrated the trends very similar to those in the case of bEnd.3 cells, but the impact of darifenacin on PEI−PLGA internalization became weaker (statistically nonsignificant in confocal image quantification analysis) (Figure S4a−d). This may provide another implication to the participation of the M3 receptor in the interaction with the PEI-based nanoparticle surface.

Theoretical Computation Identified Specific Modes of Interaction between PEI Polymer Segments and the M3 Receptor. Due to their critical roles in basic physiological processes, the muscarinic acetylcholine receptors have long been developed as targets for small molecule drug design. Several antagonists and agonists of the M3 receptor have already been approved by the FDA for treating diseases related to tissues with abundant M3 receptor expression, such as the submandibular salivary gland, bladder, or the respiratory system.[31] These drugs include M3 receptor antagonists darifenacin and tiotropium, both used as bladder relaxants, and agonist cevimeline, a drug for dry mouth syndrome.[32−34] A key element that mediates their binding with the M3 receptor has been identified through the tertiary amine moiety in their molecular structure,[35] which is also present in abundance in the structure of the branched PEI chain (Figure 1). In fact, tertiary amine nitrogen-containing molecular templates have already been used to generate potential muscarinic antagonists.[36] Using molecular dynamics simulation, a previous study has investigated the interaction between the M3 receptor and small molecule drug tiotropium and has identified multiple amino acids as being critical for such binding, including Tyr529, Tyr148, and Tyr506, which together form an aromatic

https://doi.org/10.1021/acscentsci.1c01083
ACS Cent. Sci. 2021, 7, 1938−1948

cage surrounding the ligand, together with Asp147 and Trp503, which interact with the ligand amine group.[29]

To explore whether the affinity of PEI-based nanoparticles to M3 receptor-expressing cells and tissues was also related to a similar molecular basis, we investigated the binding modes between PEI−PLGA nanoparticles and the M3 receptor through theoretical simulations. When the complexity of the whole nanoparticles used for the molecular docking simulations was considered, PEI monomer, trimer, and pentamer were used as a simplification for the outer or superficial moieties on a branched PEI-based nanoparticle surface, while the PEG monomer (ethylene glycol) and small molecule M3 antagonist tiotropium were also studied for comparison. Here, the predicted tiotropium-M3 receptor binding mode resembles the experimental crystal structure,[29] which proves the reliability of the molecular docking simulation.

The predicted binding modes by the molecular docking simulation between the studied compounds and the M3 receptor revealed a notable difference among PEI segments and PEG monomer while interacting with the protein (Figure 4a,b). All the three PEI segments (monomer, trimer, and pentamer) were shown to prefer to dock into the orthosteric binding pocket of the M3 receptor, which is actually the same binding site reported for tiotropium. When its stronger hydrophilicity was considered, the PEG monomer was predicted to interact with the M3 receptor more likely at its hydrophilic surface rather than being "inserted" into the buried orthosteric binding site. The identification of the amino acid residues of the receptor that commonly interact with these PEI segments, especially trimer and pentamer, showed a strong overlap with those that have been suggested to be critical in the M3 receptor binding with tiotropium, such as Asp147, Tyr529, Tyr506, and Ala235 (Figure 4c). None of these amino acids have been predicted to interact with the PEG monomer. The binding energy of the PEG fragment was still lower than that of the PEI fragment. The monomer, trimer, and pentamer of PEI interact with the M3 receptor at a binding energy of −2.99, −3.82, and −4.04 kCal/mol, respectively, while the PEG monomer only had a small binding energy of −1.78 kCal/mol. We speculated that, while the PEG polymer tended to form random coils under physiological conditions, a similar process was greatly hindered for PEI due to the weaker N−H···N intramolecular hydrogen bonding compared to O−H···O and the electrostatic repelling between positively charged quaternary ammonium groups. Therefore, the functional groups on a PEI-based nanoparticle surface, even if not at the terminal of the polymer chains, are expected to be more accessible than those on a PEG surface, where terminal groups are often buried in the coiled polymer. This difference, which cannot be reflected in our approximations described above, may further contribute to the disparity between the protein-binding abilities of the PEI and PEG nanoparticles in the experiment.

The strength of the interactions between the PEI segments and each of the amino acid residues in the M3 receptor were further investigated using *in silico* alanine-scanning mutagenesis (428 residues in total; Figure 4d,e). Using k-means centered cluster analysis (Figure 4d,e), it could be demonstrated that the mutation energy profiles of the three PEI segments were all grouped with that of tiotropium while being quite different from that of the PEG monomer. As shown in the destabilizing mutation energy heat map (Figure 4d), hardly any particularly strong interaction was identified between the PEG monomer and the amino acids in the M3 receptor, indicating a weak molecular docking. Instead, most of the residues that had the strongest binding with tiotropium were also predicted with high mutation energy (0.5 kCal/mol) in the interactions between PEI segments and the protein, including Asn507, Trp199, Trp503, Asp147, Tyr148, and Tyr506, implying a strong interaction of the protein with these oligomers as well as a binding mode similar to that of tiotropium-M3 receptor binding. The key amino acids in the identified PEI oligomer−M3 receptor interactions were also consistent with molecular docking predictions. As we hypothesized, these computation results agreed well with our animal and cell experiments and suggested a possible molecular basis of the M3 receptor affinity with PEI−PLGA nanoparticles.

Safety Statement. No unexpected or unusually high safety hazards were encountered.

CONCLUSION AND PERSPECTIVES

In this work, we discovered the innate targeting property of the PEI−PLGA nanoparticles toward the submandibular gland via a specific receptor−ligand interaction. Investigations on the cells further suggested this intrinsic affinity was mediated by the M3 receptor, a subtype of the acetylcholine muscarinic receptor critical to the normal function of several organs. Possible modes of molecular interaction between PEI polymer and M3 receptor have been predicted by the molecular docking simulation, implying strong binding at the orthosteric binding site of the receptor protein.

In the current study, the unique targeting property of the PEI−PLGA nanoparticles toward the submandibular gland was attributed to the specific binding affinity of the triethylamine groups toward the M3 receptor. Our results indicated the M3 receptor is also overexpressed in other organs such as brain (Figure S2). However, few PEI−PLGA nanoparticles were observed in brain (Figure 2a). The possible reason is that the intact blood−brain barrier hinders the penetration of the PEI−PLGA nanoparticles into brain. On the other hand, other muscarinic receptor subtypes (mainly M1 receptor) are also overexpressed in the submandibular gland. The selectivity of the PEI−PLGA nanoparticle toward these subtypes could also be further studied. Since the triethylamine groups on the surface of the PEI−PLGA nanoparticles are also indispensable parts in both agonists (e.g., darifenacin and solifenacin) and inhibitors (e.g., cevimeline) of the M3 receptor, the downstream signaling pathway changes of the M3 receptor after the interaction with the PEI-based nanoparticles should be clarified in the future. As reported, salivary secretion in the submandibular gland can be significantly influenced by the activation of the M3 receptor, which is regulated by the endogenous ligand of the M3 receptor, acetylcholine. However, in our preliminary experiment, no obvious change in salivary secretion was found in PEI−PLGA nanoparticle treated mice within 24 h (data not shown). Further ingenious experiments could be designed to demonstrate the influence of the PEI−PLGA nanoparticles on the M3 receptor involved signaling pathways as well as its biological function.

This discovery inspires us to explore the innate properties of commonly used nanobiomaterials, such as liposomes consisting of various lipid components,[37] nature protein nanostructures,[38] polymeric nanoparticles,[39] etc. Compared to the well-designed nanomaterials with targeted modification, these commonly used nanobiomaterials have long been favored in the pharmaceutical industry for their good pharmaceutical

https://doi.org/10.1021/acscentsci.1c01083
ACS Cent. Sci. 2021, 7, 1938−1948

performance and super cost-effectiveness. The deep understanding of their innate biological properties could also provide mechanism explanations on their *in vivo* bioactivity and side effects as well as offer guidance on further optimization of nanomedicine design. For example, nanoparticles with a cationic surface have been widely used for protein[40] or gene[41] delivery. Although the cationic surface of the nanomaterials is usually associated with high toxicity, e.g., hepatic damage and proinflammatory response,[42] a variety of cationic nanoparticles have come into the clinic for their reliability in drug loading capacity[13] and cellular endocytosis. In practice, fine-tuning the surface charge on these nanoparticles by optimizing parameters such as tail saturation and pK_a could minimize their toxicity.[13] Although the biological impact of this muscarinic receptor affinity of PEI-based nanoparticles is still to be fully evaluated, this study has provided an example that probing the molecular interactions between polymers and proteins may help us to construct polymeric nanoparticles with intrinsic biological activities and therefore extends the application potential in nanomedicine. Such strategies may help to deepen our knowledge about nano−bio interactions and provide new inspirations for the rational design of nanomedicine.

MATERIALS AND METHODS

Materials. PEI−PLGA (A−B−A triblock copolymer; PEI M_w = 25 000 (1° N: 2° N: 3° N = 4:3:4); PLGA M_w = 36 000 Da; molar ratio of D,L-lactic to glycolic acid 75:25) and mPEG−PLGA (PEG M_w = 5000; PLGA M_w = 15 000, molar ratio of D,L-lactic to glycolic acid 75:25) copolymers were purchased from Nuodepaisen Medical Technology (Suzhou, China). Fluorescent dyes Cy5.5 and Rhodamine B were purchased from Solarbio (Beijing, China) and Sigma-Aldrich (St. Louis, USA) respectively. Umbilical vein endothelium (HUVEC) and cerebral cortex microvascular endothelium (bEnd.3) cells were purchased from the Type Culture Collection Committee of the Chinese Academy of Sciences (Shanghai, China).

Preparation and Characterization of the Nanoparticles. PEI−PLGA nanoparticles were prepared by a double emulsion method as described previously.[43] Briefly, 20 mg of PEI−PLGA was fully dissolved in 1 mL of CH_2Cl_2 to which 0.2 mL of dd H_2O was added. For fluorescence imaging studies, water-soluble Cy5.5 or Rhodamine B was dissolved in this inner aqueous phase. After sonication at 35 W power for 5 min, 2 mL of an aqueous solution containing 2% poly(vinyl alcohol) was added to the mixture. The emulsion was sonicated for another 5 min and then dispersed into a 0.6% poly(vinyl alcohol) solution under stirring. The remaining organic solvent was removed by rotary evaporation. Nanoparticles were collected by centrifugation at 13 000*g* for 10 min, washed twice, and resuspended in water or saline for further use. The same method was also applied for the preparation of the PEG−PLGA nanoparticles. The hydrodynamic size and zeta potential of the prepared nanoparticles were measured by a ZetaSizer Nano series Nano-ZS (Malvern Instruments). The morphology of the nanoparticles was characterized using an HT-7700 transmission electron microscope (Hitachi) after 1% uranyl acetate staining for 4 min on copper 200-mesh grids.

Animal Maintenance. All animal uses were approved by the Committee on the Institutional Animal Care and Use Committee of the National Center for Nanoscience and Technology. Male BALB/c mice (18−20 g, 6−8 weeks) were purchased from Vital River Animal Laboratories and kept under a SPF (specific pathogen free) environment with food and water *ad libitum*.

***Ex Vivo* Imaging of PEI−PLGA Nanoparticles.** Free Rhodamine B, Rhodamine B-labeled PEI−PLGA nanoparticles, and Rhodamine B-labeled PEG−PLGA nanoparticles were intravenously injected into BALB/c mice (n = 3). The fluorescence intensities (552 nm excitation and 588 nm emission) of the three formulations were adjusted to be the same on a spectrophotometer (F-4600 FL spectrophotometer, Hitachi, Japan). All the mice were sacrificed at 8 h post-injection. Submandibular salivary glands and other major organs, including liver, kidney, spleen, lung, heart, thymus gland, and brain, were dissected and imaged using a fluorescence imaging system (Spectrum CT, PerkinElmer).

Immunofluorescence Assay. The submandibular salivary gland tissues derived from mice administered with free dye or PEI−PLGA and PEG−PLGA nanoparticles as described above was fixed in 4% paraformaldehyde, dehydrated in 15% sucrose, embedded in OCT embedding medium (cat#4583, Sakura), and cut into 8−10 μm thick slices by a freezing microtome (CRYOSTAR NX50, Thermo. with Leica 819 blades). Frozen sections were subsequently immunostained with antimuscarinic acetylcholine receptor M3 antibody (cat# ab126168, Abcam) and with fluorescence-conjugated secondary antibody (cat# GB25303, Alexa Fluor 488). The sections were also stained with 4′,6-diamidino-2-phenylindole (DAPI) to visualize the nucleus. Fluorescent images were obtained using a confocal laser scanning microscope (Lumencor light engine, Lumencor, Inc.).

Ultrathin Sections for Transmission Electron Microscopy. Submandibular salivary glands were dissected into pieces with a volume < 1 mm^3 and fixed in 2.5% glutaraldehyde overnight. The specimen was then washed 20 times with phosphate buffer, followed by postfixation with 1% osmic acid for 2 h. After washing the specimen with phosphate buffer again for 20 times, gradient dehydration was performed with 50%, 70%, 80%, 90%, and 100% alcohol solutions in ddH_2O, a 50% alcohol solution in acetone, and 100% acetone for 20 min per solution. After that, the specimen was sequentially permeated in gradient dilutions (1:1 to 1:2) of acetone and embedding reagent for 2 h, respectively, at room temperature. Then, the embedding reagent was transferred into a higher concentration for another 3 days at 4 °C. The samples were then incubated at increasing temperatures from 37 to 60 °C for 3 days using a program and maintained at 60 °C for another day. Ultrathin sections with a thickness of ∼50−100 nm were obtained by a slicer. After uranyl acetate and lead citrate staining on copper 200-mesh grids, samples were subject to HT-7700 TEM visualization.

Cell Culture and Western Blot Analysis of M3 Receptor Expression. All cells were cultured in Dulbecco's modified Eagle's medium (DMEM) supplemented with 10% heat-inactivated fetal bovine serum and 1% penicillin/streptomycin at 37 °C and 5% CO_2. For protein extraction, the cells were seeded onto 6-well plates (∼10^6 cells per well) and grown to ∼85% confluence. Subsequently, cells were washed twice with PBS and harvested with trypsin-EDTA solution (0.05% trypsin and 0.53 mmol l^{-1} EDTA). RIPA buffer (Solarbio, Beijing, China) containing 1 mM phenylmethanesulfonyl fluoride (PMSF; Solarbio, Beijing, China) was used as lysis buffer, and the protein extracts were collected

https://doi.org/10.1021/acscentsci.1c01083
ACS Cent. Sci. 2021, 7, 1938−1948

in the supernatant after centrifugation at 13 000*g* for 25 min and collected in the aqueous phase. Proteins extracted from different cells were then electrophoresed on 12% sodium dodecyl sulfate-polyacrylamide gels and transferred onto a poly(vinylidene fluoride) (PVDF) membrane. After blockage with 5% bovine serum albumin (BSA) solution for 2 h (room temperature), the PVDF membranes were incubated overnight at 4 °C with an antimuscarinic acetylcholine receptor M3 antibody (cat# ab126168, Abcam) or a rabbit polyclonal antibody against GAPDH (cat# 10494-1-AP, Proteintech). Membranes were washed four times with Tris-buffered saline containing 0.5% Tween 20 (Solarbio, China) and then incubated with HRP conjugated goat antirabbit IgG for 1 h at room temperature. The blots are treated with Super Signal West Pico Chemiluminescent Substrate (Thermo Scientific, Rockford, USA) and imaged using a ChemiDoc Touch Imaging System (Bio-Rad, USA). The bands were quantified using ImageJ 1.4.3.67 software.

Confocal Microscopy. For confocal microscopy, bEnd.3 or HUVEC cells were seeded onto 6 cm confocal observation dishes at 1×10^4 cells per dish in 1 mL of DMEM (10% fetal bovine serum) and incubated for 12 h. For the M3 receptor inhibition study, the cells were pretreated with 10 μM M3 receptor antagonist darifenacin for 1 h. Then, the medium was removed, and Cy5.5 labeled PEI−PLGA or PEG−PLGA nanoparticles (1 mg/mL) dispersed in DMEM without serum (pH 7.4 or 10.0) were added. After 0.5 h of coincubation at 4 °C, the cells were washed three times, fixed with 4% paraformaldehyde for 30 min at room temperature, and sequentially labeled with DiO for 15 min and Hoechst 33342 (buffer dsDNA) for 5 min. Confocal images were acquired by a Zeiss LSM 710 confocal microscope.

Flow Cytometry. Cells (bEnd.3 or HUVEC) were seeded into 12-well plates at 2×10^5 cells per well in 1 mL of DMEM (10% serum) and incubated for more than 12 h and pretreated with darifenacin for 1 h if needed. Nanoparticles labeled with Cy5.5 were added in DMEM without serum (1 mg mL^{-1}) at pH 7.4 or 10.0 and coincubated for 0.5 h under room temperature. The cells were washed three times and resuspended with 1 mL of PBS for flow cytometry analysis (BD Accuri C6, BD, USA). A total of 10 000 events were collected for each sample. Each treatment was performed with four replicates.

DFT Calculation and Molecular Docking Simulation. For molecular docking simulation, three PEI segments (monomer, trimer, and pentamer) together with PEG segments (monomer) and tiotropium were optimized at CHARMm force field.[44] All primary amines of PEI were protonated to model the neutral aqueous environment.[30] The protein structure of the M3 receptor was download from the Protein Data Bank database (PDB ID: 4DAJ).[45] The molecular docking simulation based on the Lamarckian Genetic Algorithm between these ligands and M3 receptor[29] was performed by Autodock 4.2.6 software.[46] Panels of mutants for *in silico* alanine-scanning mutagenesis were generated using BIOVIA Discovery Studio 2018. The mutation energy was predicted for all the 428 individual amino acid residues of the monomer of the M3 receptor. Cluster analysis on the mutation energy of different amino acids was carried out by the k-means method with Cluster 3.0 (Stanford University) and was visualized with Java Treeview (Stanford University).

Statistical Analysis. Statistical analysis was performed using SPSS Statistics 19.0.0. For multiple comparisons, one-way analysis of variance followed with a Tukey posthoc test was performed. For comparison between two groups, Student's *t* test was used. All data are presented as mean ± SD in which $p < 0.05$ was considered statistically significant (*, $p < 0.05$; **, $0.001 < p < 0.01$; ***, $p < 0.001$).

■ ASSOCIATED CONTENT

Supporting Information

The Supporting Information is available free of charge at https://pubs.acs.org/doi/10.1021/acscentsci.1c01083.

Characterization and stability test of the nanoparticles; TEM image; M3 receptor expression; affinity test on the HUVEC cell line (PDF)

■ AUTHOR INFORMATION

Corresponding Authors

Guangjun Nie − *CAS Key Laboratory for Biomedical Effects of Nanomaterials & Nanosafety, Laboratory of Theoretical and Computational Nanoscience, CAS Center for Excellence in Nanoscience, National Center for Nanoscience and Technology, Beijing 100190, China; University of Chinese Academy of Sciences, Beijing 100049, P. R. China;* orcid.org/0000-0001-5040-9793; Email: niegj@nanoctr.cn

Yinlong Zhang − *School of Nanoscience and Technology, University of Chinese Academy of Sciences, Beijing 100049, China*; Email: zhangyinlong@ucas.ac.cn

Authors

Junchao Xu − *CAS Key Laboratory for Biomedical Effects of Nanomaterials & Nanosafety, Laboratory of Theoretical and Computational Nanoscience, CAS Center for Excellence in Nanoscience, National Center for Nanoscience and Technology, Beijing 100190, China; University of Chinese Academy of Sciences, Beijing 100049, P. R. China*

Kaiwei Wan − *CAS Key Laboratory for Biomedical Effects of Nanomaterials & Nanosafety, Laboratory of Theoretical and Computational Nanoscience, CAS Center for Excellence in Nanoscience, National Center for Nanoscience and Technology, Beijing 100190, China; University of Chinese Academy of Sciences, Beijing 100049, P. R. China;* orcid.org/0000-0001-8518-6550

Hui Wang − *CAS Key Laboratory for Biomedical Effects of Nanomaterials & Nanosafety, Laboratory of Theoretical and Computational Nanoscience, CAS Center for Excellence in Nanoscience, National Center for Nanoscience and Technology, Beijing 100190, China; University of Chinese Academy of Sciences, Beijing 100049, P. R. China*

Xinghua Shi − *CAS Key Laboratory for Biomedical Effects of Nanomaterials & Nanosafety, Laboratory of Theoretical and Computational Nanoscience, CAS Center for Excellence in Nanoscience, National Center for Nanoscience and Technology, Beijing 100190, China; University of Chinese Academy of Sciences, Beijing 100049, P. R. China;* orcid.org/0000-0001-5012-3453

Jing Wang − *CAS Key Laboratory for Biomedical Effects of Nanomaterials & Nanosafety, Laboratory of Theoretical and Computational Nanoscience, CAS Center for Excellence in Nanoscience, National Center for Nanoscience and Technology, Beijing 100190, China; University of Chinese Academy of Sciences, Beijing 100049, P. R. China*

Yi Zhong − *State Key Laboratory of Natural and Biomimetic Drugs, School of Pharmaceutical Sciences, Peking University, Beijing 100191, China*

Chao Gao − *CAS Key Laboratory for Biomedical Effects of Nanomaterials & Nanosafety, Laboratory of Theoretical and Computational Nanoscience, CAS Center for Excellence in Nanoscience, National Center for Nanoscience and Technology, Beijing 100190, China; University of Chinese Academy of Sciences, Beijing 100049, P. R. China*

Complete contact information is available at: https://pubs.acs.org/10.1021/acscentsci.1c01083

Author Contributions

[#]J.X. and K.W. contributed equally to this work.

Notes

The authors declare no competing financial interest.

■ ACKNOWLEDGMENTS

All authors appreciate the efforts made by Prof. Bin Li from NCNST for providing the results of PEI−PLGA self-assembly by the DPD simulation method. G.N. and Y. Zhang acknowledge grants from the National Basic Research Plan of China (2018YFA0208900), the Key Research Program of Frontier Sciences CAS (ZDBS-LY-SLH039), and K. C. Wong Education Foundation (GJTD-2018-03).

■ REFERENCES

(1) Wang, J.; Li, Y.; Nie, G. Multifunctional biomolecule nanostructures for cancer therapy. *Nature Reviews Materials* **2021**, *6*, 766.

(2) Dubacheva, G. V.; Curk, T.; Auzély-Velty, R.; Frenkel, D.; Richter, R. P. Designing multivalent probes for tunable superselective targeting. *Proc. Natl. Acad. Sci. U. S. A.* **2015**, *112* (18), 5579.

(3) Ulijn, R. V.; Smith, A. M. Designing peptide based nanomaterials. *Chem. Soc. Rev.* **2008**, *37* (4), 664.

(4) Farokhzad, O. C.; Cheng, J. J.; Teply, B. A.; Sherifi, I.; Jon, S.; Kantoff, P. W.; Richie, J. P.; Langer, R. Targeted nanoparticle-aptamer bioconjugates for cancer chemotherapy in vivo. *Proc. Natl. Acad. Sci. U. S. A.* **2006**, *103* (16), 6315.

(5) Li, S. P.; Jiang, Q.; Liu, S. L.; Zhang, Y. L.; Tian, Y. H.; Song, C.; Wang, J.; Zou, Y. G.; Anderson, G. J.; Han, J. Y.; et al. A DNA nanorobot functions as a cancer therapeutic in response to a molecular trigger in vivo. *Nat. Biotechnol.* **2018**, *36* (3), 258.

(6) Yuan, Y.; Du, C.; Sun, C. J.; Zhu, J.; Wu, S.; Zhang, Y. L.; Ji, T. J.; Lei, J. L.; Yang, Y. M.; Gao, N.; et al. Chaperonin-GroEL as a Smart Hydrophobic Drug Delivery and Tumor Targeting Molecular Machine for Tumor Therapy. *Nano Lett.* **2018**, *18* (2), 921.

(7) Ji, T. J.; Lang, J. Y.; Ning, B.; Qi, F. F.; Wang, H.; Zhang, Y. L.; Zhao, R. F.; Yang, X.; Zhang, L. J.; Li, W.; et al. Enhanced Natural Killer Cell Immunotherapy by Rationally Assembling Fc Fragments of Antibodies onto Tumor Membranes. *Adv. Mater.* **2019**, *31* (6), 1804395.

(8) Mizrahy, S.; Peer, D. Polysaccharides as building blocks for nanotherapeutics. *Chem. Soc. Rev.* **2012**, *41* (7), 2623.

(9) Min, Y. Z.; Caster, J. M.; Eblan, M. J.; Wang, A. Z. Clinical Translation of Nanomedicine. *Chem. Rev.* **2015**, *115* (19), 11147.

(10) Barenholz, Y. Doxil (R) - The first FDA-approved nano-drug: Lessons learned. *J. Controlled Release* **2012**, *160* (2), 117.

(11) Duncan, R. The dawning era of polymer therapeutics. *Nat. Rev. Drug Discovery* **2003**, *2* (5), 347.

(12) Richards Grayson, A. C.; Doody, A. M.; Putnam, D. Biophysical and structural characterization of polyethylenimine-mediated siRNA delivery in vitro. *Pharm. Res.* **2006**, *23* (8), 1868.

(13) Han, X.; Mitchell, M. J.; Nie, G. Nanomaterials for Therapeutic RNA Delivery. *Matter* **2020**, *3* (6), 1948.

(14) Lyu, Z.; Peng, L. Potent drugless dendrimers. *Nature Biomedical Engineering* **2017**, *1* (9), 686.

(15) Al-Jamal, K. T.; Al-Jamal, W. T.; Akerman, S.; Podesta, J. E.; Yilmazer, A.; Turton, J. A.; Bianco, A.; Vargesson, N.; Kanthou, C.; Florence, A. T.; et al. Systemic antiangiogenic activity of cationic poly-L-lysine dendrimer delays tumor growth. *Proc. Natl. Acad. Sci. U. S. A.* **2010**, *107* (9), 3966.

(16) Kang, S.-g.; Zhou, G.; Yang, P.; Liu, Y.; Sun, B.; Huynh, T.; Meng, H.; Zhao, L.; Xing, G.; Chen, C.; et al. Molecular mechanism of pancreatic tumor metastasis inhibition by $Gd@C_{82}(OH)_{22}$ and its implication for de novo design of nanomedicine. *Proc. Natl. Acad. Sci. U. S. A.* **2012**, *109* (38), 15431.

(17) Thomas, M.; Klibanov, A. M. Conjugation to gold nanoparticles enhances polyethylenimine's transfer of plasmid DNA into mammalian cells. *Proc. Natl. Acad. Sci. U. S. A.* **2003**, *100* (16), 9138.

(18) Liu, Y.; Wu, D. C.; Zhang, W. D.; Jiang, X.; He, C. B.; Chung, T. S.; Goh, S. H.; Leong, K. W. Polyethylenimine-grafted multiwalled carbon nanotubes for secure noncovalent immobilization and efficient delivery of DNA. *Angew. Chem., Int. Ed.* **2005**, *44* (30), 4782.

(19) Zhang, S. F.; Kucharski, C.; Doschak, M. R.; Sebald, W.; Uludag, H. Polyethylenimine-PEG coated albumin nanoparticles for BMP-2 delivery. *Biomaterials* **2010**, *31* (5), 952.

(20) Zhang, Y.; Han, X.; Nie, G. Responsive and activable nanomedicines for remodeling the tumor microenvironment. *Nat. Protoc.* **2021**, *16* (1), 405.

(21) Bin, L.; You-Liang, Z.; Dan, X.; Han-Wen, P.; Hong, L. Computer Simulation of Vesicle Structure from Self-assembly of Miktoarm Star-like Block Copolymers in Dilute Solution. *Chem. J. Chinese Universities* **2013**, *34* (7), 1667.

(22) Duff, M. O.; Olson, S.; Wei, X.; Garrett, S. C.; Osman, A.; Bolisetty, M.; Plocik, A.; Celniker, S. E.; Graveley, B. R. Genome-wide identification of zero nucleotide recursive splicing in Drosophila. *Nature* **2015**, *521*, 376.

(23) Yamada, M.; Miyakawa, T.; Duttaroy, A.; Yamanaka, A.; Moriguchi, T.; Makita, R.; Ogawa, M.; Chou, C. J.; Xia, B.; Crawley, J. N.; et al. Mice lacking the M3 muscarinic acetylcholine receptor are hypophagic and lean. *Nature* **2001**, *410* (6825), 207.

(24) Poulin, B.; Butcher, A.; McWilliams, P.; Bourgognon, J. M.; Pawlak, R.; Kong, K. C.; Bottrill, A.; Mistry, S.; Wess, J.; Rosethorne, E. M.; et al. The M-3-muscarinic receptor regulates learning and memory in a receptor phosphorylation/arrestin-dependent manner. *Proc. Natl. Acad. Sci. U. S. A.* **2010**, *107* (20), 9440.

(25) Dragunow, M. M-3 muscarinic receptors as targets for drug development in neurodegenerative disorders. *Nat. Rev. Drug Discovery* **2008**, *7* (2), 185.

(26) Gautam, D.; Jeon, J.; Starost, M. F.; Han, S. J.; Hamdan, F. F.; Cui, Y. H.; Parlow, A. F.; Gavrilova, O.; Szalayova, I.; Mezey, E.; et al. Neuronal M-3 muscarinic acetylcholine receptors are essential for somatotroph proliferation and normal somatic growth. *Proc. Natl. Acad. Sci. U. S. A.* **2009**, *106* (15), 6398.

(27) Georgieva, J. V.; Kalicharan, D.; Couraud, P. O.; Romero, I. A.; Weksler, B.; Hoekstra, D.; Zuhorn, I. S. Surface Characteristics of Nanoparticles Determine Their Intracellular Fate in and Processing by Human Blood-Brain Barrier Endothelial Cells In Vitro. *Mol. Ther.* **2011**, *19* (2), 318.

(28) Radu, B. M.; Osculati, A. M. M.; Suku, E.; Banciu, A.; Tsenov, G.; Merigo, F.; Di Chio, M.; Banciu, D. D.; Tognoli, C.; Kacer, P.; et al. All muscarinic acetylcholine receptors (M-1-M-5) are expressed in murine brain microvascular endothelium. *Sci. Rep.* **2017**, *7*, 5083.

(29) Kruse, A. C.; Hu, J. X.; Pan, A. C.; Arlow, D. H.; Rosenbaum, D. M.; Rosemond, E.; Green, H. F.; Liu, T.; Chae, P. S.; Dror, R. O.; et al. Structure and dynamics of the M3 muscarinic acetylcholine receptor. *Nature* **2012**, *482* (7386), 552.

(30) Qu, F.; Li, N. B.; Luo, H. Q. Highly Sensitive Fluorescent and Colorimetric pH Sensor Based on Polyethylenimine-Capped Silver Nanoclusters. *Langmuir* **2013**, *29* (4), 1199.

(31) Abrams, P.; Andersson, K. E.; Buccafusco, J. J.; Chapple, C.; de Groat, W. C.; Fryer, A. D.; Kay, G.; Laties, A.; Nathanson, N. M.; Pasricha, P. J.; et al. Muscarinic receptors: their distribution and

function in body systems, and the implications for treating overactive bladder. *Br. J. Pharmacol.* **2006**, *148* (5), 565.
(32) Sorbera, L. A.; Castaner, J. Cevimeline hydrochloride - Treatment of Sjogren's Syndrome muscarinic M-1 and M-3 agonist. *Drugs Future* **2000**, *25* (6), 558.
(33) Beroukas, D.; Goodfellow, R.; Hiscock, J.; Jonsson, R.; Gordon, T. P.; Waterman, S. A. Up-regulation of M3-muscarinic receptors in labial salivary gland acini in primary Sjogren's syndrome. *Lab. Invest.* **2002**, *82* (2), 203.
(34) Fife, R. S.; Chase, W. F.; Dore, R. K.; Wiesenhutter, C. W.; Lockhart, P. B.; Tindall, E.; Suen, J. Y. Cevimeline for the treatment of xerostomia in patients with Sjogren syndrome - A randomized trial. *Arch. Intern. Med.* **2002**, *162*, 1293.
(35) Peretto, I.; Petrillo, P.; Imbimbo, B. P. Medicinal chemistry and therapeutic potential of muscarinic M3 antagonists. *Med. Res. Rev.* **2009**, *29* (6), 867.
(36) Tumiatti, V.; Minarini, A.; Milelli, A.; Rosini, M.; Buccioni, M.; Marucci, G.; Ghelardini, C.; Bellucci, C.; Melchiorre, C. Structure−activity relationships of methoctramine-related polyamines as muscarinic antagonist: Effect of replacing the inner polymethylene chain with cyclic moieties. *Bioorg. Med. Chem.* **2007**, *15* (6), 2312.
(37) Cheng, Q.; Wei, T.; Farbiak, L.; Johnson, L. T.; Dilliard, S. A.; Siegwart, D. J. Selective organ targeting (SORT) nanoparticles for tissue-specific mRNA delivery and CRISPR-Cas gene editing. *Nat. Nanotechnol.* **2020**, *15* (4), 313.
(38) Gaudet, R. G.; Zhu, S.; Halder, A.; Kim, B. H.; Bradfield, C. J.; Huang, S.; Xu, D.; Maminska, A.; Nguyen, T. N.; Lazarou, M. A human apolipoprotein L with detergent-like activity kills intracellular pathogens. *Science* **2021**, *373*, 6552.
(39) Shao, S.; Zhou, Q.; Si, J.; Tang, J.; Liu, X.; Wang, M.; Gao, J.; Wang, K.; Xu, R.; Shen, Y. A non-cytotoxic dendrimer with innate and potent anticancer and anti-metastatic activities. *Nat. Biomed Eng.* **2017**, *1* (9), 745.
(40) Li, S.; Zhang, Y.; Wang, J.; Zhao, Y.; Ji, T.; Zhao, X.; Ding, Y.; Zhao, X.; Zhao, R.; Li, F.; et al. Nanoparticle-mediated local depletion of tumour-associated platelets disrupts vascular barriers and augments drug accumulation in tumours. *Nat. Biomed Eng.* **2017**, *1* (8), 667.
(41) Wang, B.; Ding, Y.; Zhao, X.; Han, X.; Yang, N.; Zhang, Y.; Zhao, Y.; Zhao, X.; Taleb, M.; Miao, Q. R.; et al. Delivery of small interfering RNA against Nogo-B receptor via tumor-acidity responsive nanoparticles for tumor vessel normalization and metastasis suppression. *Biomaterials* **2018**, *175*, 110.
(42) Landesman-Milo, D.; Peer, D. Toxicity profiling of several common RNAi-based nanomedicines: a comparative study. *Drug Delivery Transl. Res.* **2014**, *4* (1), 96.
(43) Wang, H.; Zhao, Y.; Wu, Y.; Hu, Y. L.; Nan, K.; Nie, G.; Chen, H. Enhanced anti-tumor efficacy by co-delivery of doxorubicin and paclitaxel with amphiphilic methoxy PEG-PLGA copolymer nanoparticles. *Biomaterials* **2011**, *32* (32), 8281.
(44) Momany, F. A.; Rone, R.; et al. Validation of the general purpose QUANTA ®3.2/CHARMm® force field. *J. Comput. Chem.* **1992**, *13* (7), 888.
(45) Berman, H. M.; Westbrook, J.; Feng, Z.; Gilliland, G.; Bhat, T. N.; Weissig, H.; Shindyalov, I. N.; Bourne, P. E. The Protein Data Bank. *Nucleic Acids Res.* **2000**, *28* (1), 235.
(46) Morris, G. M.; Huey, R.; Lindstrom, W.; Sanner, M. F.; Belew, R. K.; Goodsell, D. S.; Olson, A. J. AutoDock4 and AutoDockTools4: Automated Docking with Selective Receptor Flexibility. *J. Comput. Chem.* **2009**, *30* (16), 2785.

https://doi.org/10.1021/acscentsci.1c01083
ACS Cent. Sci. 2021, 7, 1938−1948